AGU PUBLICATIONS

Geophysical Research Letters

RESEARCH LETTER
10.1002/2014GL060060

**Key Points:**
- The postspinel transition is consistent with the 660 discontinuity
- The Clapeyron slope of the postspinel boundary is −2.5 MPa/K
- Discrepancy in the previous studies is likely due to technical issues

**Supporting Information:**
- Readme
- Figure S1
- Table S1
- Table S2
- Table S3
- Table S4

**Correspondence to:**
Y. Ye,
yuye1@asu.edu

**Citation:**
Ye, Y., C. Gu, S.-H. Shim, Y. Meng, and V. Prakapenka (2014), The postspinel boundary in pyrolitic compositions determined in the laser-heated diamond anvil cell, *Geophys. Res. Lett.*, *41*, 3833–3841, doi:10.1002/2014GL060060.

Received 27 MAR 2014
Accepted 21 MAY 2014
Accepted article online 26 MAY 2014
Published online 11 JUN 2014

# The postspinel boundary in pyrolitic compositions determined in the laser-heated diamond anvil cell

**Yu Ye[1], Chen Gu[2], Sang-Heon Shim[1], Yue Meng[3], and Vitali Prakapenka[4]**

[1]School of Earth and Space Exploration, Arizona State University, Tempe, Arizona, USA, [2]Department of Earth, Atmospheric, and Planetary Sciences, Massachusetts Institute of Technology, Cambridge, Massachusetts, USA, [3]HPCAT, Carnegie Institution of Washington, Argonne, Illinois, USA, [4]GeoSoilEnviroCARS, University of Chicago, Chicago, Illinois, USA

**Abstract** In situ multianvil press (MAP) studies have reported that the depth and the Clapeyron slope of the postspinel boundary are significantly less than those of the 660 km discontinuity inferred from seismic studies. These results have raised questions about whether the postspinel transition is associated with the discontinuity. We determined the postspinel transition in pyrolitic compositions in the laser-heated diamond anvil cell (LHDAC) combined with in situ synchrotron X-ray diffraction. The Clapeyron slope was determined to be −2.5 ± 0.4 MPa/K and did not vary significantly with compositions and used pressure scales. Using Pt scales, our data indicate that the postspinel transition occurs in pyrolitic compositions at 23.6–24.5 GPa (1850 K). The transition pressure and slope are consistent with the depth and topography of the 660 km discontinuity. Our data reveal that inaccuracy in pressure scales alone cannot explain the discrepancy and technical differences between MAP and LHDAC contribute significantly to the discrepancy.

## 1. Introduction

The origin of a global seismic velocity discontinuity at a depth of 660 km (hereafter called the 660 discontinuity) has been the focus of studies for the properties and the behavior of the mantle, such as convection, chemical structure, and chemical mixing. Earlier quench studies in multianvil press (MAP) showed that the postspinel phase transition occurs at the pressure expected for the depth of the 660 discontinuity [e.g., *Ito and Takahashi*, 1989]. However, the first in situ MAP experiments on $Mg_2SiO_4$ suggested that the postspinel transition occurs at a depth 50 km shallower than the discontinuity [*Irifune et al.*, 1998]. The majority of subsequent in situ MAP experiments have not only confirmed the shallower transition but also suggested that the Clapeyron slope is considerably smaller (−0.4 to −1.3 MPa/K) or even positive (0.6 to 1.2 MPa/K) [*Katsura et al.*, 2003; *Fei et al.*, 2004a; *Litasov et al.*, 2005; *Ghosh et al.*, 2013]. The Clapeyron slope has been also reported in quench MAP studies, −1.0 MPa/K [*Ishii et al.*, 2011] to −2.8 MPa/K [*Hirose*, 2002], but pressures were not determined at in situ high pressure–temperature (*P*–*T*) conditions. By assuming that the lateral variation of the depth of the 660 discontinuity is caused by the thermal response of a phase transition, seismic studies have suggested a substantially greater slope of −2.5 to −3.0 MPa/K [*Lebedev et al.*, 2002; *Fukao et al.*, 2009], which is not consistent with the results of in situ MAP studies. The mismatch between experimental studies and seismic observations requires other explanations for the origin of the 660 discontinuity, such as the postgarnet transition [*Hirose et al.*, 2001] and the effect of water [*Ghosh et al.*, 2013].

In contrast, a laser-heated diamond anvil cell (LHDAC) study reported a depth of the boundary that is consistent with the 660 discontinuity [*Shim et al.*, 2001] using a shockwave-based Pt scale [*Holmes et al.*, 1989]. The study also suggested that inaccuracy in the pressure scales might be an important source of the discrepancies in MAP studies. Many studies have attempted to improve the accuracy of the pressure scales. Updated Au scales that combine a wide range of data [*Fei et al.*, 2007; *Dorogokupets and Oganov*, 2007; *Yokoo et al.*, 2009] yield pressures that are 0.6–1.8 GPa higher than those obtained from MAP studies that used the Au scale by *Anderson et al.* [1989]. However, the magnitude of this change is not sufficient to match the transition depth and the Clapeyron slope measured in MAP to the 660 discontinuity. In this study, we report new data sets on the postspinel transition in pyrolitic compositions that were determined in LHDAC.

## 2. Experimental Procedures

Two starting materials, $MgO–Al_2O_3–SiO_2$ (MAS) and $CaO–MgO–Al_2O_3–SiO_2–FeO$ (CMASF), were synthesized using the laser levitation method [*Tangeman et al.*, 2001] with oxide ratios of the pyrolitic composition [*McDonough and Sun*, 1995]. For the Fe-bearing sample, we ensured the reducing conditions during glass synthesis by using a mixture of $CO/CO_2$ gas. Electron microprobe analysis indicated average compositions of 46.3 ± 0.6 wt % MgO, 5.1 ± 0.1 wt % $Al_2O_3$, and 48.4 ± 0.4 wt % $SiO_2$ for MAS, and 3.9 ± 0.1 wt % CaO, 39.2 ± 1.0 wt % MgO, 4.6 ± 0.1 wt % $Al_2O_3$, 43.7 ± 1.1 wt % $SiO_2$, and 8.6 ± 0.2 wt % FeO for CMASF. Three separate mixtures were prepared: MAS + Pt (Pt from Aldrich, >99.9 %, 0.5–1.2 μm grain size), MAS + Au (Au from Aldrich, >99.9 %, 1.5–3.0 μm grain size), and CMASF + Au with a weight ratio of 9:1. Au or Pt was used as both an internal pressure standard and a laser coupler. Due to the alloying of Au and Pt, these two pressure standards were never loaded together. We did not mix Pt with CMASF because of the reaction between Fe-bearing silicates and Pt to form Pt-Fe alloy [*Rubie*, 1999].

Diamond anvils with 400 μm culets were aligned in a short symmetric-type diamond anvil cell (DAC). A Re gasket was preindented to a thickness of 30–35 μm with a 260 μm hole. A cold-pressed thin foil (~200 × 100 × 10 $\mu m^3$) of a sample + metal mixture was loaded with 3 or 4 spacer particles (<10 μm) on each side of the culet to prop up the foil during the cryogenic loading of liquid Ar to form Ar layers that separated the foil from the diamond anvils for thermal insulation during laser heating. The spacers had the same compositions as the foil but did not contain Pt or Au. In order to prevent capturing of $H_2O$, the loading was conducted in a dry Ar chamber where the Ar gas pressure was maintained higher than the atmospheric pressure throughout the procedure. In Raman scattering measurements, no detectable amount of $H_2O$ has been found in an Ar medium [e.g., *Catalli et al.*, 2008].

Synchrotron X-ray diffraction (XRD) patterns were measured in situ at high *P–T* in double-sided LHDAC at beamline 13-IDD of the GeoSoilEnviroConsortium for Advanced Radiation Sources (GSECARS) sector [*Prakapenka et al.*, 2008] and beamline 16-IDB of the High Pressure Collaborative Access Team (HPCAT) sector [*Meng et al.*, 2006] at the Advanced Photon Source. Monochromatic X-ray beams (GSECARS: $\lambda = 0.3344$ Å and beam size = 3 × 4 μm; HPCAT: $\lambda = 0.3515$ Å and beam size = 5 × 6 μm) were focused on the sample with MarCCD detectors to measure the diffraction images. Near-infrared laser beams were focused on the sample with a hot spot size of 20–25 μm and were aligned coaxially with the X-ray beam. A membrane push plate was attached to the DAC, so that we could adjust the pressure of the sample in the DAC with a precision of ~0.2 GPa. Thermal radiation spectra from both sides of the sample were measured using an imaging spectrometer simultaneously with XRD patterns and fitted to the Planck black-body equation to obtain temperatures.

In a typical run cycle, a previously unheated fresh amorphous spot on the sample foil was chosen for heating to avoid kinetics problems. XRD measured before heating confirmed that the unheated regions were amorphous (see Figure S1 in the supporting information). The laser power was increased quickly to reach the target temperature within 1 min. Six to 12 diffraction patterns were taken during a heating cycle of 15–30 min. The heating duration is comparable to those in previous in situ MAP studies, 5–90 min [*Irifune et al.*, 1998; *Katsura et al.*, 2003; *Litasov et al.*, 2005; *Ghosh et al.*, 2013]. Diffraction peaks from crystalline phases typically appeared within ~5 min of heating, and no further changes were detected in the diffraction patterns after ~8 min of heating, suggesting the formation of a stable phase assemblage (see Figure S1). Seven to 15 heating run cycles were performed at different spots in each foil.

Some LHDAC studies observed phase transitions along both forward and reverse directions by heating of crystalline phases [e.g., *Shim et al.*, 2001]. This method may less likely result in synthesis of metastable assemblages, but it could suffer from slow diffusion through the grain boundaries of crystalline phases. Instead, heating of amorphous starting materials should suffer much less from the kinetic issues [*Grocholski et al.*, 2012]. The properties of the postspinel transition in MAS measured using heating of amorphous starting material agree well with those in $Mg_2SiO_4$ measured using reversal heating on crystalline phases [*Shim et al.*, 2001] when the same Pt scales are used.

The software package fit2D [*Hammersley et al.*, 1996] was used to reduce the diffraction images to diffraction patterns. The phase identification was conducted by the software XPEAKPO [*Shim*, 2007], and the diffraction peaks were fitted with pseudo-Voigt profile functions to obtain the peak positions. The data obtained from the GSECARS and HPCAT beamlines agreed well with each other.

To cross calibrate the Au and Pt pressure scales, we conducted similar measurements on Pt + MgO and Au + MgO mixtures in the LHDAC at the synchrotron. MgO powder (from Aldrich, >99.999 %) was dried at ~800 K for 24 h, and mixed with 10 wt % Pt or Au powder. The same experimental methods as described above were applied.

## 3. Results and Discussions

In situ XRD patterns measured during laser heating provide a direct means to identify stable phases at different *P*–*T* conditions (Figures 1a–1d). When they coexists, some ringwoodite (Rw) peaks overlap with the garnet (Gt) peaks. However, Rw can be typically identified by the 400, 333, and 440 peaks, whereas Gt can be distinguished by the 024, 224, 134, 026, and 046 peaks. The 200 and 220 lines are diagnostic for ferropericlase (Fp), although the 111 peak overlaps with the perovskite (Pv) 112 and 200 peaks. Some akimotoite (Ak) peaks also overlap with the Pv peaks. However, Ak can still be identified by the 104, 110, $11\bar{6}$, and 300 peaks. Pv can be easily identified by its characteristic doublets at 002 + 110 and 004 + 220, as well as other peaks (e.g., 111, 211, 023, 221, 114, and 132), although a triplet at 020 + 112 + 200 overlaps with the Ar and Fp peaks. In CMASF, Ca-perovskite (Ca-Pv) can be distinguished by lines 200, 211, and 111, whereas the most intense line, 110, overlaps with the Ar line. For Pt or Au, 3 or 4 lines (111, 200, 220, and 311) can be indexed to obtain unit cell parameters.

The pressures were calculated using the Au (blue symbols) and Pt (red symbols) scales of *Fei et al.* [2007] (hereafter Au-F07 and Pt-F07, respectively), which are based on a cross comparison of the unit cell volumes of Au and Pt in MAP [*Fei et al.*, 2004b]. The pressure and temperature for each data point are the average values of several diffraction patterns and thermal radiation spectra, respectively, taken during the heating cycle with $1\sigma$ uncertainties from the standard deviations. The difference in the calculated pressures between the 111 and 200 diffraction lines of Au and Pt is generally less than 1 GPa. The temperature difference from both sides of the sample foil is generally less than 100 K.

In both MAS and CMASF, the postspinel boundary can be determined by changes in the observed phases from Rw + Gt to Pv + Fp (Figures 2a and 2b) (see Table S1). At higher temperatures, Rw breaks down to Pv + Fp before the post-Gt transition. In a few heating cycles, we observed low-*P* (Ak + Gt + Rw) and high-*P* (Pv + Fp) phase assemblages together (light-colored symbols), which indicates that the *P*–*T* conditions may correspond to those of the postspinel boundary. In MAS, Ak was observed at a pressure slightly above the postspinel transition at $T \leq 1800$ K (squares in Figure 2a), whereas the high-*P* stability of Ak was not observed in CMASF. Ak was observed at temperatures as high as 2300 K in MAS but was not observed at $T \geq 2050$ K in CMASF (these data will be presented elsewhere). These differences may be related to the compositional differences between MAS and CMASF (e.g., Fe).

In MAS, the postspinel transition (Rw out) occurred at 23.7 and 24.5 GPa (1850 K) on the Pt scales of *Dorogokupets and Oganov* [2007] and *Fei et al.* [2007], respectively (Figure 2a). However, for the same starting material (MAS) but with the Au standard, the transition occurred at 25.8 and 27.8 GPa (1850 K) on the *Anderson et al.* [1989] and *Fei et al.* [2007] scales, respectively, which is 2.1–3.3 GPa higher than the same boundary for the same composition when determined with Pt. In CMASF, we only used the Au standard because of the possible contamination of Pt in Fe-bearing silicates; the postspinel transition occurred at 25.7–27.7 GPa (1850 K) with the Au scales. The difference in pressure of the phase boundary in MAS using Pt and Au indicates inaccuracy in the pressure scales.

We corrected the pressures determined by Au-F07 with respect to Pt-F07 by −3.3 GPa so that the two MAS boundaries that were determined separately with the Pt and Au scales match each other. The same correction constant was also applied to the CMASF boundary. Figures 2c and 2d illustrate that none of the recently improved Au scales match the postspinel boundary measured in the MAP with the 660 discontinuity within a reasonable temperature range (1800–2000 K). However, all of the recently updated Pt scales display good agreement between the boundary measured in the LHDAC and the 660 discontinuity, including the scale that is independent of the preexisting pressure scales [*Yokoo et al.*, 2009] (the boundary with the Yokoo scale is between the two red lines in Figures 2c and 2d). Among the MAP data, the phase boundary in $Mg_2SiO_4$ reported by *Fei et al.* [2004a] based on the MgO scale of *Speziale et al.* [2001] (hereafter MgO-S01) is the closest to the 660 discontinuity. However, our study indicates that the postspinel transition pressure in $Mg_2SiO_4$ is 0.2~1.0 GPa higher than that in pyrolitic compositions, likely due to the effect of Fe. The Fe effect we found is similar to those reported in quench MAP studies [*Ito and Takahashi*, 1989; *Ishii et al.*, 2011].

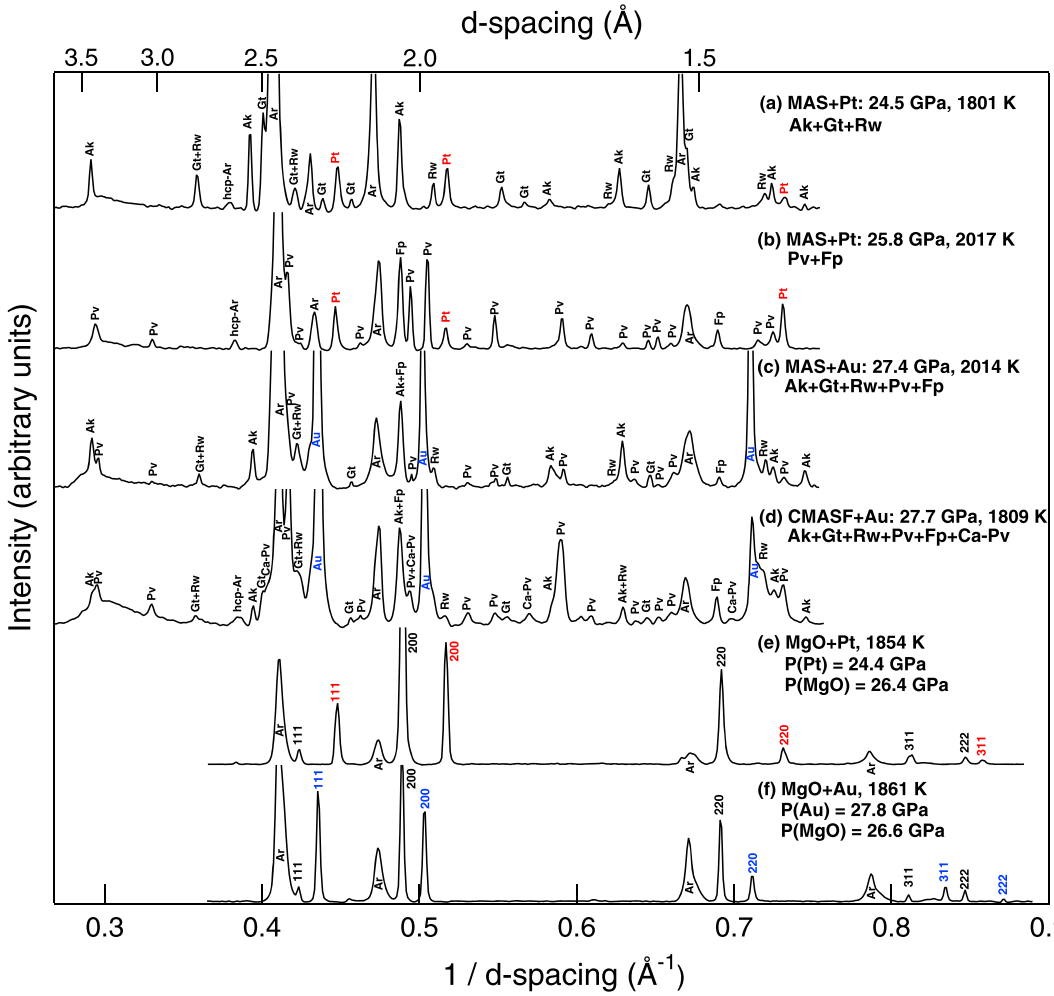


**Figure 1.** X-ray diffraction patterns of (a and b) MAS + Pt, (c) MAS + Au, (d) CMASF + Au, and (e and f) pressure standard mixtures at high *P–T*. Diffraction patterns shown in Figures 1a and 1b display peaks from the phases below and above the postspinel transition, respectively. Figures 1c and 1d display peaks from both low- and high-*P* phase assemblages, including akimotoite (Ak), garnet (Gt), ringwoodite (Rw), perovskite (Pv), and ferropericlase (Fp). Argon (Ar) was loaded for pressure transmission and thermal insulation. The red, blue, and black indices in Figures 1e and 1f are peaks from Pt, Au, and MgO, respectively. The background subtracted diffraction intensities are plotted as a function of the inverse of the interplanar distance (*d* spacing).

Although determining the absolute pressure of the postspinel transition is challenging, our data sets based on both Au and Pt provide robust constraints on the Clapeyron slope of the postspinel transition, because the determination relies on relative scales. The Clapeyron slope of the postspinel transition in both MAS and CMASF has been measured as $-2.5 \pm 0.4$ MPa/K across the wide range of Pt and Au scales considered (see Table S2). This finding suggests that Fe does not affect the slope. Our slope is measured over a wide temperature range that includes both Rw + Gt → Pv + Fp at lower *T* and Rw → Pv + Fp at higher *T*. Although the change in the phase assemblage may affect the slope, we did not find any significant changes within our experimental resolution. Therefore, the slope reported here should be regarded as the "Rw-out" boundary.

The slopes that we obtained in the LHDAC are consistent with seismic estimates from the observed topography of the 660 discontinuity, which are −2.5 to −3.0 MPa/K [*Lebedev et al.*, 2002; *Fukao et al.*, 2009], and are significantly different from those reported in situ MAP experiments, 1.2 to −1.3 MPa/K [*Katsura et al.*, 2003; *Ghosh et al.*, 2013; *Litasov et al.*, 2005; *Fei et al.*, 2004a]. Even if we use the same Au scales, we still find a considerably steeper slope of −2.4 to −2.8 MPa/K in the LHDAC, which indicates that the gentle slope observed in MAP studies cannot be attributed entirely to the pressure scale issue.

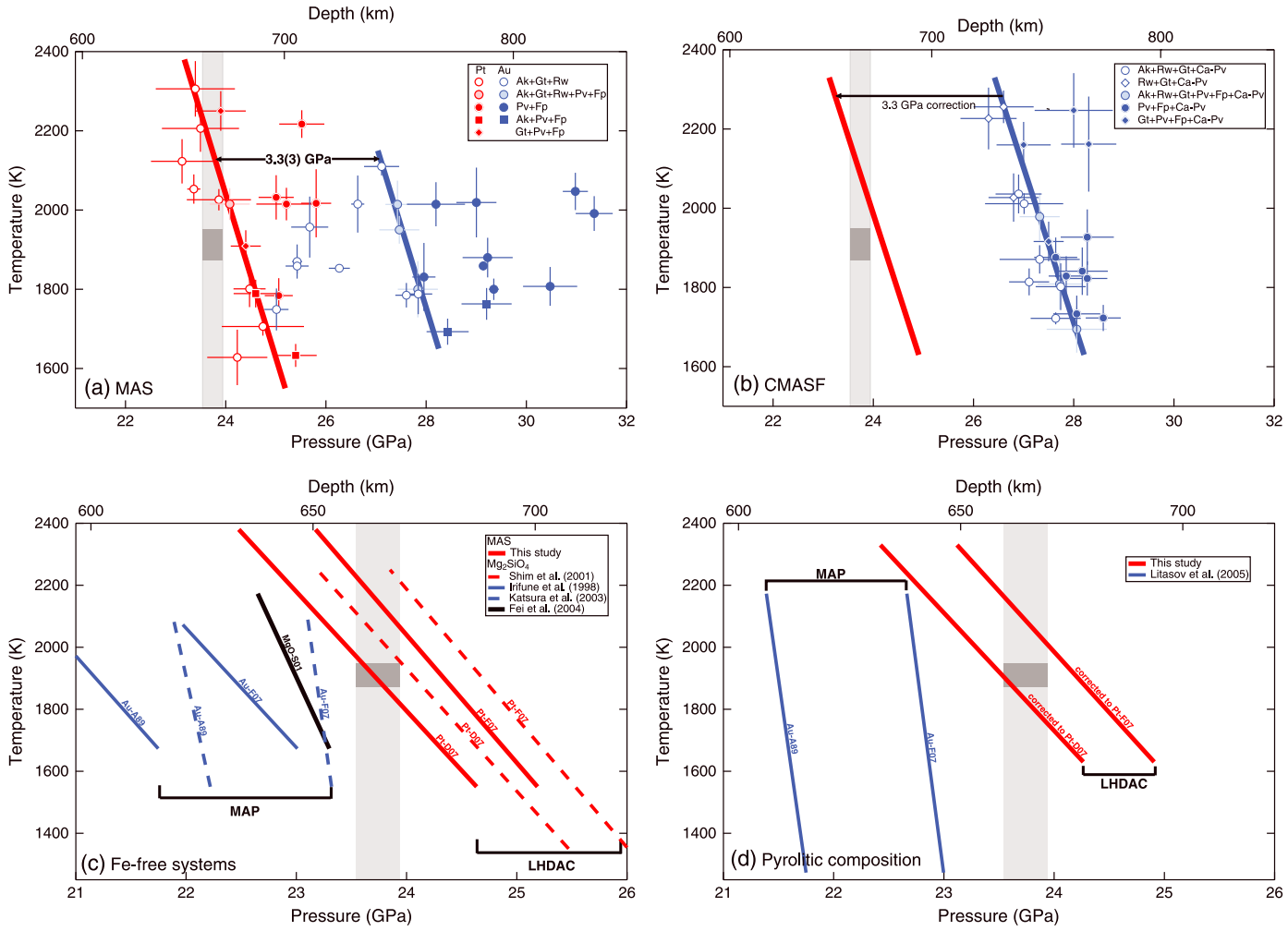


**Figure 2.** The postspinel boundary in (a) MAS and (b) CMASF determined on the Pt (red symbols and lines) and Au (blue symbols and lines) scales of *Fei et al.* [2007] . The error bars are 1$\sigma$ uncertainties. Comparisons of in situ measurements are made between LHDAC (this study and *Shim et al.* [2001]) and MAP [*Irifune et al.*, 1998; *Katsura et al.*, 2003; *Litasov et al.*, 2005] in (c) Fe-free samples and (d) pyrolitic samples. The phase boundary in $Mg_2SiO_4$ of *Ghosh et al.* [2013] (not shown here) occurs at a slightly lower pressure (0.3 GPa) and a similar Clapeyron slope to that of *Katsura et al.* [2003]. The light gray vertical bar represents the pressure expected for the 660 discontinuity from the ak135_f [*Kennett et al.*, 1995] and Preliminary Reference Earth Model (PREM) [*Dziewonski and Anderson*, 1981] models, and the depths on the top axis are also calculated from the ak135_f model. The dark gray box indicates the temperature range suggested by *Brown and Shankland* [1981] and *Stacey* [1992] at the 660 discontinuity. Au-A89 is the Au scale by *Anderson et al.* [1989].

To further examine the pressure scale issue, we conducted in situ XRD on pressure standard mixtures at *P–T* conditions comparable to those of the MAS and CMASF experiments. The unit cell volumes of MgO, Au, and Pt were calculated from four to five diffraction lines from among 111, 200, 220, 311, and 222 (Figures 1e and 1f). We only used the data that exhibited temperature gradients of less than 100 K and pressure differences of less than 1 GPa between the 111 and 200 peaks. We calculated pressures from Pt-F07, Au-F07, and MgO-S01. The uncertainties in *T* and *V* were also propagated to the uncertainty in *P* (see Tables S3 and S4).

Figure 3a illustrates that Au-F07 overestimates the pressures by 0.9 ± 0.4 GPa with respect to MgO-S01, whereas Pt-F07 underestimates the pressures by 1.9 ± 0.6 GPa at 1500–2200 K and 20–31 GPa. These two observations indicate that Au-F07 overestimates pressures by 2.8 ± 0.7 GPa compared with Pt-F07, which is consistent with the discrepancy between Pt and Au scales that we found for the postspinel transition in MAS (3.3 ± 0.3 GPa). The discrepancy might increase with temperature for Pt (Figure 3a), but such increasing magnitude is less than the resolution of our technique for the relatively narrow temperature range of the measurement. The pressures measured at 300 K after heating (Figure 3a) using Au-F07, Pt-F07, and MgO-S01 agreed within ±0.5 GPa. Such agreement suggests that the 3 GPa discrepancy is mainly caused by uncertainties in the thermal parts of the equations of state (EoSs).

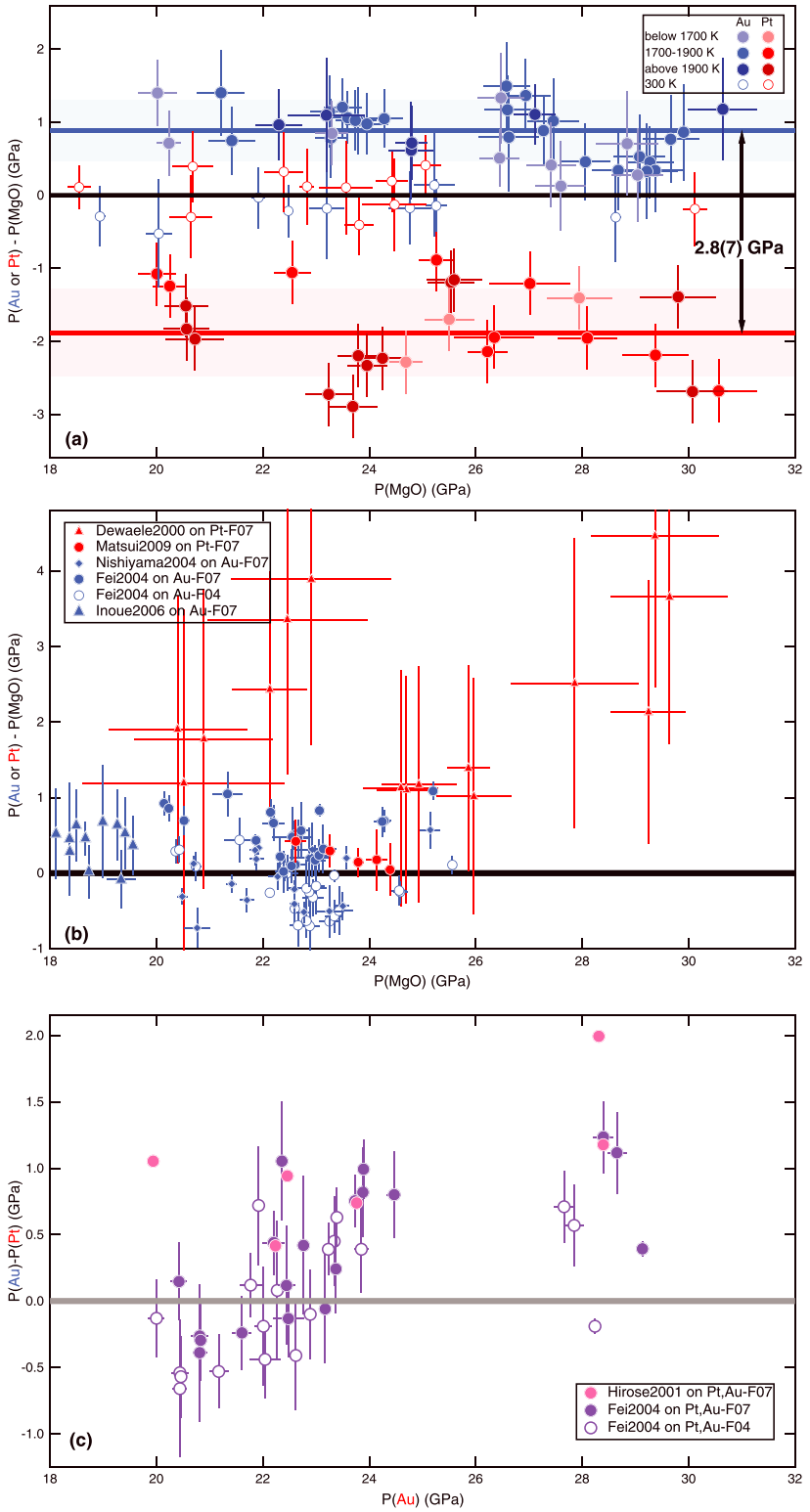


**Figure 3.** Pressure differences between the Au (blue)/Pt (red) pressure standards and MgO identified from (a) the data from this study at 1500–2200 K (solid symbols) and 300 K (open symbols) and (b) other studies [*Dewaele et al.*, 2000; *Fei et al.*, 2004b; *Nishiyama et al.*, 2004; *Inoue et al.*, 2006; *Matsui et al.*, 2009]. (c) Direct comparison between Au and Pt [*Hirose et al.*, 2001; *Fei et al.*, 2004b]. We used MgO-S01, Au-F07, and Pt-F07 for the pressure calculations, except for the open symbols in Figures 3b and 3c, which were calculated using the scales of *Fei et al.* [2004b]. The error bars are $1\sigma$ uncertainties. The average differences in pressure are shown as the horizontal lines with $1\sigma$ uncertainties (light-colored areas) in Figure 3a. Pt-F04 and Au-F04 are the Pt and Au scales of *Fei et al.* [2004b], respectively.

Although the magnitude of discrepancy between Au and Pt standards varies depending on chosen scales, Au scales systematically overestimate pressures with respect to Pt scales. If we apply other recent scales that include data with electronic contributions to the EoSs [*Dorogokupets and Oganov*, 2007; *Yokoo et al.*, 2009], the Au scales still predict pressures that are 1.4–2.8 GPa higher than those estimated with the Pt scales.

Figure 3b presents the pressure differences between Au/Pt and MgO in existing data sets. Whereas the data of *Nishiyama et al.* [2004] indicate that there is no difference between the Au-F07 and MgO-S01 scales, the plot illustrates that Au-F07 results in an average difference of ~0.5 GPa from MgO-S01 for the MAP data by *Fei et al.* [2004b] and *Inoue et al.* [2006], which is similar to our LHDAC results for the same scales. *Dewaele et al.* [2000] reported MgO + Pt data measured in LHDAC at 1750–2500 K (Figure 3b). Their data indicate an opposite trend (i.e., the Pt-F07 scale predicts higher pressures than the MgO-S01 scale) to our results. However, the data scatter (±1.8 GPa) is considerably larger than our results (±0.5 GPa). The MAP data of *Matsui et al.* [2009] indicate that there is no difference between Pt-F07 and MgO-S01.

The MAP data of *Fei et al.* [2004b] indicate agreement between Au-F07 and Pt-F07 at pressures below 24 GPa, but above 24 GPa, the pressures obtained by Au-F07 are ~1 GPa higher than those predicted by Pt-F07 (Figure 3c). Furthermore, the MAP data of *Hirose et al.* [2001] indicate that the pressures obtained by Au-F07 are approximately 0.5–2 GPa higher than those predicted by Pt-F07, which is similar to our LHDAC results of 2.8 ± 0.7 GPa. In summary, the discrepancy that we observed between Au-F07 and Pt-F07 is also present in some MAP data [*Fei et al.*, 2004b; *Hirose et al.*, 2001; *Inoue et al.*, 2006], which justifies the need to correct the pressure scales.

It is also important to note that MgO-S01 used the Pt + MgO data of *Dewaele et al.* [2000], which are significantly different from our Pt + MgO data and the pressure was calculated using the Pt scale of *Holmes et al.* [1989]. The 300 K isotherm of the Pt scale was shown to be inaccurate by a static compression study in the DAC with He medium [*Dewaele et al.*, 2004]. The effects may have propagated to Au-F07 and Pt-F07 (but to different degrees) because they were constructed based on MgO-S01 and Au-F07, respectively.

The comparison of the Clapeyron slope measured in MAP and LHDAC showed that the pressure scale issue cannot be the only cause of the discrepancy. Additionally, when the Au scale of *Anderson et al.* [1989] is applied to our LHDAC data, we obtain a postspinel transition pressure of 25.6–25.8 ± 0.2 GPa at 1850 K. At the same temperature and using the same Au scale, MAP studies have reported a postspinel transition pressure of 21.3–22.0 GPa in $Mg_2SiO_4$ [*Irifune et al.*, 1998; *Katsura et al.*, 2003] and 21.5 GPa in pyrolite [*Litasov et al.*, 2005]. These findings indicate that there is a difference of at least 3.6 GPa between the MAP and LHDAC results, even if the same pressure scale is used. Therefore, the technical differences between MAP and LHDAC should contribute significantly to the discrepancies in the depth and Clapeyron slope of the postspinel boundary that are measured using those techniques.

Important technical differences include thermal gradients and temperature measurements. Although thermal gradient remains an important source of error in LHDAC [*Kavner and Panero*, 2004], we reduce it by conducting double-side heating, using much smaller the sizes of X-ray beams than those of hot spots, and insulating the samples thermally in an Ar medium. Since metals directly couple with laser beams, whereas Fe-free samples (such as MgO) do not, Au and Pt may be at higher temperature than MgO in the LHDAC. If the 2 GPa discrepancy between MgO and Pt (Figure 3a) is entirely due to temperature gradients, MgO should be ~250 K cooler than Pt within the area measured by X-ray. However, our Au + MgO comparison is consistent with the MAP data of *Fei et al.* [2004b]. Because Fe in CMASF couples directly with the laser beams, the problem should be much smaller at least in CMASF. Therefore, the thermal gradient in LHDAC may not be the main source of the discrepancy. The measured temperature in MAP may also include some uncertainties because of the temperature gradient, the pressure effect on the thermocouple calibration, and diffraction from materials in cold spots [*Rubie*, 1999; *Nishiyama et al.*, 2004].

In situ MAP studies have used energy-dispersive XRD for phase identification [*Irifune et al.*, 1998; *Katsura et al.*, 2003; *Fei et al.*, 2004a; *Litasov et al.*, 2005; *Ghosh et al.*, 2013]. The detection of small part of the Debye diffraction rings in the method could lead to problems in phase identification and therefore determination of phase boundaries. *Shim et al.* [2001] reported strong preferred orientation during the postspinel transition. We used angle-dispersive XRD which measures full Debye rings.

Although it is unclear which of the Pt and Au scales are accurate, our LHDAC data in pyrolitic compositions, which were calculated using recent Pt scales, provide a depth and Clapeyron slope of the postspinel

boundary that are consistent with seismic observations of the 660 discontinuity. However, none of the recent Au scales reconcile the discrepancy in the depth and slope of the postspinel boundary between the MAP results and seismic observations. If the postspinel transition is responsible for the 660 discontinuity as suggested by our new data, then a compositional change across the 660 discontinuity is not required. Whereas accuracy of pressure scales remains an important issue, as revealed by our new data, future mineral physics studies should address systematic error sources in MAP and LHDAC for reliable comparisons between laboratory data and seismic observations.

**Acknowledgments**

We thank two anonymous reviewers for their helpful comments. Discussions with Kurt Leinenweber improved this paper. This work was supported by NSF grants EAR1316007 and EAR1301813 to S.H.S. The synchrotron experiments were conducted at GSECARS and HPCAT, Advanced Photon Source (APS), and Argonne National Laboratory. GSECARS is supported by NSF-Earth Science (EAR-1128799) and DOE-GeoScience (DE-FG02-94ER14466). HPCAT is supported by DOE-NNSA (DE-NA0001974), DOE-BES (DE-FG02-99ER45775), and NSF. A.P.S. is supported by DOE-BES, under contract DE-AC02-06CH11357.

The Editor thanks two anonymous reviewers for their assistance in evaluating this paper.

## References

Anderson, O. L., D. G. Issak, and S. Yamamoto (1989), Anharmonicity and the equation of state for gold, *J. Appl. Phys.*, *65*, 1534–1543.

Brown, J. M., and T. J. Shankland (1981), Thermodynamic parameters in the Earth as determined from seismic profiles, *Geophys. J. R. Astron. Soc.*, *66*, 579–596.

Catalli, K., S.-H. Shim, and V. B. Prakapenka (2008), A crystalline-to-crystalline phase transition in $Ca(OH)_2$ at 8 GPa and room temperature, *Geophys. Res. Lett.*, *35*, L05312, doi:10.1029/2007GL033062.

Dewaele, A., G. Fiquet, D. Andrault, and D. Hausermann (2000), P-V-T equation of state of periclase from synchrotron radiation measurements, *J. Geophys. Res.*, *105*(B2), 2869–2877.

Dewaele, A., P. Loubeyre, and M. Mezouar (2004), Equation of state of six metals above 94 GPa, *Phys. Rev. B*, *70*, 094112.

Dorogokupets, P. I., and A. R. Oganov (2007), Ruby, metals, and MgO as alternative pressure scales: A semiempirical description of shockwave, ultrasonic, x-ray, and thermochemical data at high temperatures and pressures, *Phys. Rev. B*, *75*, 024115.

Dziewonski, A. M., and D. L. Anderson (1981), Preliminary reference Earth model, *Phys. Earth Planet. Inter.*, *25*, 297–356.

Fei, Y., J. van Orman, J. Li, W. van Westrenen, C. Sanloup, W. Minarik, K. Hirose, T. Komabayashi, M. Walter, and K. Funakoshi (2004a), Experimentally determined postspinel transformation boundary in $Mg_2SiO_4$ using MgO as an internal pressure standard and its geophysical implications, *J. Geophys. Res.*, *109*, B02305, doi:10.1029/2003JB002562.

Fei, Y., J. Li, K. Hirose, W. Minarik, J. V. Orman, C. Sanloup, W. van Westrenen, T. Komabayashi, and K.-I. Funakoshi (2004b), A critical evaluation of pressure scales at high temperatures by in situ X-ray diffraction measurements, *Phys. Earth Planet. Inter.*, *143-144*, 515–526.

Fei, Y., A. Ricolleau, M. Frank, K. Mibe, G. Shen, and V. Prakapenka (2007), Toward an internally consistent pressure scale, *Proc. Nat. Acad. Sci.*, *104*(22), 9182–9186.

Fukao, Y., M. Obayashi, T. Nakakuki, and D. S. P. Group (2009), Stagnant slab: A review, annual review, *Annu. Rev. Earth Planet. Sci.*, *37*, 19–46.

Ghosh, S., E. Ohtani, K. D. Litasov, A. Suzuki, D. Dobson, and K. Funakoshi (2013), Effect of water in depleted mantle on post-spinel transition and implication for 660 km seismic discontinuity, *Earth Planet. Sci. Lett.*, *371-372*, 103–111.

Grocholski, B., K. Catalli, S.-H. Shim, and V. Prakapenka (2012), Mineralogical effects on the detectability of the post-perovskite boundary, *Proc. Nat. Acad. Sci.*, *109*, 2275–2279.

Hammersley, A. P., S. O. Svensson, M. Hanfland, A. N. Fitch, and D. Häusermann (1996), Two-dimensional detector software: From real detector to idealised image or two-theta scan, *High Pressure Res.*, *14*, 235–248.

Hirose, K., T. Komabayashi, M. Murakami, and K. Funakoshi (2001), In situ measurements of majorite-akimotoite-perovskite phase transition boundary in $MgSiO_3$, *Geophys. Res. Lett.*, *22*, 4351–4345.

Hirose, K. (2002), Phase transitions in pyrolitic mantle around 670-km depth: Implications for upwelling of plumes from the lower mantle, *J. Geophys. Res.*, *107*(B4), ECV 3-1–ECV 3-13, doi:10.1029/2001JB000597.

Holmes, N. C., J. A. Moriarty, G. R. Gathers, and W. J. Nellis (1989), The equation of state of platinum to 660 GPa (6.6 Mbar), *J. Appl. Phys.*, *66*, 2962–2967.

Inoue, T., et al. (2006), The phase boundary between wadsleyite and ringwoodite in $Mg_2SiO_4$ determined by in situ X-ray diffraction, *Phys. Chem. Miner.*, *33*, 106–114.

Irifune, T., et al. (1998), The postspinel phase boundary in $Mg_2SiO_4$ determined by in situ x-ray diffraction, *Science*, *279*, 1698–1700.

Ishii, T., H. Kojitani, and M. Akaogi (2011), Post-spinel transitions in pyrolite and $Mg_2SiO_4$ and akimotoite-perovskite transition in $MgSiO_3$: Precise comparison by high-pressure high-temperature experiments with multi-sample cell technique, *Earth Planet. Sci. Lett.*, *309*, 185–197.

Ito, E., and E. Takahashi (1989), Postspinel transformations in the system $Mg_2SiO_4$-$Fe_2SiO_4$ and some geophysical implications, *J. Geophys. Res.*, *94*(B8), 10,637–10,646.

Katsura, T., et al. (2003), Post-spinel transition in $Mg_2SiO_4$ determined by high P-T in situ x-ray diffractometry, *Phys. Earth Planet. Inter.*, *136*, 11–24.

Kavner, A., and W. R. Panero (2004), Temperacell gradients and evaluation of thermoelastic properties in the synchrotron-based laser-heated diamond cell, *Phys. Earth Planet. Inter.*, *143-144*, 527–539.

Kennett, B. L. N., E. R. Engdahi, and R. Buland (1995), Constraints on seismic velocities in the Earth from travel times, *Geophys. J. Int.*, *122*, 108–124.

Lebedev, S., S. Chevrot, and R. D. van der Hilst (2002), Seismic evidence for olivine phase changes at the 410- and 660-kilometer discontinuities, *Science*, *296*, 1300–1302.

Litasov, K., E. Ohtani, A. Sano, A. Suzuki, and K. Funakoshi (2005), In situ x-ray diffraction study of post-spinel transformation in a peridotite mantle: Implication for the 660-km discontinuity, *Earth Planet. Sci. Lett.*, *238*, 311–328.

Matsui, M., E. Ito, T. Katsura, D. Yamazaki, T. Yoshino, A. Yokoyama, and K. i. Funakoshi (2009), The temperature-pressure-volume equation of state of platinum, *J. Appl. Phys.*, *105*, 013505, doi:10.1063/1.3054,331.

McDonough, W. F., and S.-S. Sun (1995), The composition of the Earth, *Chem. Geol.*, *120*, 223–253.

Meng, Y., G. Shen, and H. K. Mao (2006), Double-sided laser heating system at HPCAT for *insitu* x-ray differentiation at high pressures and high temperatures, *J. Phys. Condens. Matter*, *18*, S1097–S1103.

Nishiyama, N., T. Irifune, T. Inoue, J.-I. Ando, and K.-I. Funadoshi (2004), Precise determination of phase relations in pyrolite across the 660 km seismic discontinuity by in situ x-ray diffraction and quench experiments, *Phys. Earth Planet. Inter.*, *143-144*, 185–199.

Prakapenka, V. B., A. Kubo, A. Kuznetsov, A. Laskin, O. Shkurikhin, P. Dera, M. L. Rivers, and S. R. Sutton (2008), Advanced flat top laser heating system for high pressure research at GSECARS: Application to the melting behavior of germanium, *High Pressure Res.*, *28*(3), 225–235.

Rubie, D. C. (1999), Characterising the sample environment in multianvil high-pressure experiments, *Phase Transitions A Multinational J.*, *68*(3), 431–451.

Shim, S.-H (2007), Development of an X-ray diffraction analysis program suite for large data sets, COMPRES Annual Meeting.

Shim, S.-H., T. S. Duffy, and G. Shen (2001), The post-spinel transformation in $Mg_2SiO_4$ and its relation to the 660-km seismic discontinuity, *Nature*, *411*, 571–574.

Speziale, S., C.-S. Zha, T. S. Duffy, R. J. Hemley, and H. K. Mao (2001), Quasi-hydrostatic compression of magnesium oxide to 52 GPa: Implications for the pressure-volume-temperature equation of state, *J. Geophys. Res.*, *106*(B1), 515–528.

Stacey, F. D. (1992), *Physics of the Earth,* 3rd ed., Brookfield Press, Brisbane, Qld., Australia.

Tangeman, J. A., B. L. Phillips, A. Navrotsky, J. K. R. Weber, A. D. Hixson, and T. S. Key (2001), Vitreous forsterite ($Mg_2SiO_4$): Synthesis, structure, and thermochemistry, *Geophys. Res. Lett.*, *28*, 2517–2520.

Yokoo, M., N. Kawai, and K. G. Nakamura (2009), Ultrahigh pressure scales for gold and platinum at pressures up to 550 GPa, *Phys. Rev. B*, *80*, 104114.